TOXICOLOGICAL SCIENCES **92(2)**, 456–463 (2006)
doi:10.1093/toxsci/kfl020
Advance Access publication May 19, 2006

The Interaction of Manganese Nanoparticles with PC-12 Cells Induces Dopamine Depletion

Saber M. Hussain,*[,1] Amanda K. Javorina,* Amanda M. Schrand,† Helen M. Duhart,‡ Syed F. Ali,‡ and John J. Schlager*

Applied Biotechnology Branch, Human Effectiveness Directorate, Air Force Research Laboratory, Wright-Patterson AFB, Ohio 45431; †Department of Chemical and Materials Engineering, University of Dayton, Dayton, Ohio 45469; and ‡Neurochemistry Laboratory, Division of Neurotoxicology, National Center for Toxicological Research/FDA, Jefferson, Arkansas 72079

Received February 5, 2006; accepted March 25, 2006

This investigation was designed to determine whether nano-sized manganese oxide (Mn-40nm) particles would induce dopamine (DA) depletion in a cultured neuronal phenotype, PC-12 cells, similar to free ionic manganese (Mn^{2+}). Cells were exposed to Mn-40nm, Mn^{2+} (acetate), or known cytotoxic silver nanoparticles (Ag-15nm) for 24 h. Phase-contrast microscopy studies show that Mn-40nm or Mn^{2+} exposure did not greatly change morphology of PC-12 cells. However, Ag-15nm and $AgNO_3$ produce cell shrinkage and irregular membrane borders compared to control cells. Further microscopic studies at higher resolution demonstrated that Mn-40nm nanoparticles and agglomerates were effectively internalized by PC-12 cells. Mitochondrial reduction activity, a sensitive measure of particle and metal cytotoxicity, showed only moderate toxicity for Mn-40nm compared to similar Ag-15nm and Mn^{2+} doses. Mn-40nm and Mn^{2+} dose dependently depleted DA and its metabolites, dihydroxyphenylacetic acid (DOPAC) and homovanillic acid (HVA), while Ag-15nm only significantly reduced DA and DOPAC at concentrations of 50 μg/ml. Therefore, the DA depletion of Mn-40nm was most similar to Mn^{2+}, which is known to induce concentration-dependent DA depletion. There was a significant increase (> 10-fold) in reactive oxygen species (ROS) with Mn-40nm exposure, suggesting that increased ROS levels may participate in DA depletion. These results clearly demonstrate that nanoscale manganese can deplete DA, DOPAC, and HVA in a dose-dependent manner. Further study is required to evaluate the specific intracellular distribution of Mn-40nm nanoparticles, metal dissolution rates in cells and cellular matrices, if DA depletion is induced *in vivo*, and the propensity of Mn nanoparticles to cross the blood-brain barrier or be selectively uptaken by nasal epithelium.

Key Words: **nanoparticles; manganese; *in vitro* toxicity; PC-12 cells; dopamine.**

Nanotechnology involves the creation and manipulation of materials at the nanoscale level to produce unique products with novel properties. Nanomaterials, which are functionally defined as having a single-dimensional feature within the range of 1–100 nm, have been used to create materials that exhibit novel physicochemical properties and functions imparted through this engineered, controlled feature size. Nanomaterials such as nanotubes, nanowires, fullerene derivatives (buckyballs), and quantum dots have received enormous national attention for creating new consumer products as well as advancing science with novel analytical tools for both physical and life sciences (Cui and Gao, 2003; Wu and Bruchez, 2004). Examples include the synthesis and use of uniformly sized magnetic nanoparticles for magnetic storage media, ferrofluids, magnetic resonance imaging, and magnetically guided drug delivery. Nanomaterials are of interest to the Air Force because of their potential use in multiple advanced systems for applications including electronics, sensors, and energy production.

Man-made nanoparticles and materials are being rapidly produced in large quantities throughout the world. With the increased probability of exposure from large-yield industry production, the issue of toxicity has led to new investigations of dosing and exposure to elemental metals. Although a wide and growing number of applications for nanomaterials exist, there is a serious lack of information concerning the human health and environmental implications of these manufactured nanomaterials. Limited studies assessing the toxicity of man-made nanomaterials are available. These provide an initial risk assessment of nanomaterials through the extension of exposure data from research models (Braydich-Stolle *et al.*, 2005; Hussain *et al.*, 2005; Lam *et al.*, 2004; Monteiro-Riviere *et al.*, 2005; Oberdörster, 2004). Lam *et al.* (2004) demonstrated that carbon nanotube products induced dose-dependent epithelial granulomas in mouse lungs, and in some cases, deep lung interstitial inflammation occurred in the animals 7 days postexposure. A study by Oberdörster *et al.* (2005) indicated that fullerenes (C_{60}) induced oxidative stress in the fish brain. Multiwalled carbon nanotube interactions with human epidermal keratinocytes were studied by Monteiro-Riviere *et al.* (2005), who found that nanotubes produced a toxic irritant response to cells by releasing proinflammatory cytokines. However, a key issue presently overlooked in evaluating the

[1] To whom correspondence should be addressed. Fax: (937) 904-9610. E-mail: saber.hussain@wpafb.af.mil.

utility and distribution of man-made nanomaterials is assessing their potential toxicity based on their inherent chemical composition (e.g., heavy metals), diverse level of carbon-based functionalization, and/or nanoscale chemically stable properties. Therefore, further critical science-based processes must be considered to assure the safety of these nanomaterials after primary exposure, such as those encountered by individuals working with these materials, and secondary exposure by individuals such as consumers. Studies from our laboratory with *in vitro* models to evaluate potential toxicity of nanomaterials have indicated that nanomaterials such as silver (Ag-15nm and -100nm) showed significant toxicity in liver cells compared to controls (Hussain *et al.*, 2005). Recently, Ag nanoparticles have been used as antimicrobial agents and in wound care applications (Furno, 2004).

Studies on humans have indicated that elevated levels of Mn may put humans at risk of parkinsonism (Olanow, 2004). This suggests that there may be significant pathological consequences and risks to the central nervous system (CNS) when manufacturing nanoscale metals. Larger amounts of manganese metal or powder applications are typically found in industries involving steel and nonsteel alloy production, battery manufacture, colorants, pigments, ferrites, welding fluxes, fuel additives, catalysts, and metal coatings. Due to the recent development of nanomaterials, macro-sized manganese particles are likely to be replaced by manganese nanoparticles. The applications of Mn nanomaterials are currently being pursued for catalysis and battery technology (Han *et al.*, 2005).

Manganese (Mn) exposure is known to produce neurotoxicity *in vitro* and in animal models (Aschner *et al.*, 2005; Jayakumar *et al.*, 2004). *In vitro* studies provide evidence that Mn specifically targets the dopaminergic system. PC-12 cells are a neuroendocrine cell line with the capability to produce the neurotransmitter dopamine (DA) and contain functional DA metabolism pathways. The present study was conducted to determine if nano-sized manganese oxide particles can cause the depletion of DA and its metabolites, dihydroxyphenylacetic acid (DOPAC) and homovanillic acid (HVA), in PC-12 cells. We show that DA depletion occurs in a dose-dependent manner after cells are exposed to Mn-40nm nanoparticles for 24 h and that the level of disruption is quite similar to its soluble counterpart Mn^{2+}. Additionally, Mn-40nm produces high levels of reactive oxygen species (ROS) that are much greater than the levels produced by either Mn^{2+} or Ag-15nm, which suggests that DA depletion after incubation with Mn-40nm in PC-12 cells may be associated with oxidative stress.

MATERIALS AND METHODS

Chemicals. Manganese oxide (Mn-40nm) and silver (Ag-15nm) nanoparticles were generous gifts from Dr Gunter Oberdörster (University of Rochester School of Medicine and Dentistry, Rochester, NY) and Dr Karl Martin (Nanotechnology, Inc, Austin, TX), respectively. Manganese acetate, silver nitrate ($AgNO_3$), 3-(4,5-dimethylthiazol-2-yl)-2,5-diphenyltetrazolium bromide (MTT), perchloric acid, DA, DOPAC, HVA, 3,4-dihydroxybenzylamine, and penicillin/streptomycin were purchased from the Sigma Chemical Company (St Louis, MO). RPMI-1640 medium was purchased from American Type Culture Collection (ATCC, Manassas, VA). 6-Carboxy-29 and 79-dichlorofluorescin diacetate (DCFH-DA) were purchased from Molecular Probes Inc (Eugene, OR).

Cell culture. The PC-12 cell line, derived from *Rattus norvegicus* pheochromocytoma (CRL-1721), was obtained from American Type Tissue Culture (http://www.atcc.org). PC-12 cells were grown in RPMI-1640 media supplemented with 5% fetal bovine serum, 10% horse serum (both heat inactivated), and 1% penicillin/streptomycin in a humidified atmosphere with 5% CO_2 at 37°C. The cells were cultured on rat-tail collagen–coated flasks, plates, and slides. PC-12 cells are a neuroendocrine cell line with a capability to produce and excrete the neurotransmitter DA. This cell line can be used as a model cell for testing DA depletion. Cells were cultured by plating at densities to produce an 80% culture substrate confluency after 24 h when they were then used for exposure studies.

Dispersion of nanomaterials in solution. Relatively homogeneous nanoparticle dispersions (10 mg/ml stock solutions) were prepared by brief sonication (Cole-Parmer 470 50 W ultrasonic tip processor). Ag-15nm particles were dispersed in sterile deionized water and both Mn-40nm nanoparticles and Mn acetate in physiological saline. From these stock solutions, different final concentrations ranging from 1 to 100 μg/ml were prepared in cell growth medium (RPMI-1640). However, the preparation of relatively homogenous dispersions of nanomaterial dilutions from the stock solutions into cell culture media is an issue that has not yet been satisfactorily resolved. Both Ag-15nm and Mn-40nm tend to agglomerate, which may not change the chemical nature of the nanoparticles but may impact the actual size of the particle interacting with the cells and its associated cytotoxicity. The addition of a detergent such as 1% Tween-20 appears to enable homogenous dispersion (Fig. 1). However, due to the adverse effects of Tween-20 on PC-12 cell viability, this agent was not used in these experiments.

Transmission electron microscopy of Mn-40nm nanoparticles. Transmission electron microscopy (TEM) characterization was performed on a Hitachi H-7600 tungsten-tip instrument at an accelerating voltage of 120 kV. Mn-40nm nanoparticles were examined after suspension in water and subsequent deposition onto formvar/carbon-coated TEM grids. The advanced microscopy techniques software for the digital TEM camera was calibrated for size measurements of the nanoparticles. Information on mean size and SD were calculated from a random field of view in addition to images that show agglomeration and general morphology of the nanoparticles (Fig. 2).

Exposure protocol. PC-12 cells were grown for at least 24 h until they reached 80% confluency in six-well plates or two-chambered slides. They were then treated with 1–100 μg/ml of nanoparticles suspended in culture growth medium. After 24 h of incubation, multiple toxicity end points were evaluated in control and nanoparticle-exposed cells.

Microscopic studies for morphological changes and uptake of nanoparticles. After PC-12 cells were exposed to various concentrations of nanoparticles or soluble metal (Mn^{2+}, $AgNO_3$) for 24 h, cells (control and exposed) were washed with PBS, slide chambers removed, coverslips placed on the slides, and the edges of the coverslips sealed with clear nail polish to avoid the movement of coverslips while examining under the microscope. Morphological changes were observed with phase-contrast inverted microscopy at 20× magnification (Fig. 3). Uptake and interaction of Mn-40nm were also examined on an Olympus inverted light microscope modified with the CytoViva150 Ultra Resolution Imaging (URI) system with advanced optical illumination at ×60 (Fig. 4). This improved the microscope resolution in order to observe particles as small as 100 nm in size. The microscope pictures were captured by using QCapture Pro Imaging software.

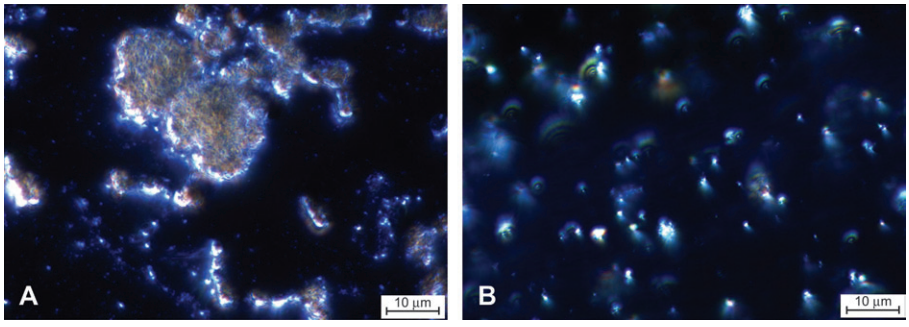

FIG. 1. Mn-40nm nanoparticle dispersion in physiological solutions observed with advanced high-illuminating microscopy. Dispersed nanoparticles (1 mg/ml) were examined with an Olympus IX71 Microscope platform coupled to the CytoViva150 URI system and show that Mn-40 nanoparticles suspended with 1% Tween have increased dispersion compared to Mn-40 in physiological saline. (A) Mn-40nm 60× normal; (B) Mn-40nm 60× + 1% Tween.

Cytotoxicity end points. Cell viability was determined by the MTT assay for mitochondrial function (Carmichael *et al.*, 1987) with a slight modification, which is based on the conversion of tetrazolium salt into an insoluble formazan product by various dehydrogenases in mitochondria. PC-12 cells were plated at approximately 1 million cells/ml, grown to 80% confluency, and exposed to various concentrations of nanoparticles (1–100 µg/ml) for 24 h. At the end of incubation, cells were treated with the MTT solution (final concentration, 1 mg/ml) for 30 min at 37°C in a cell culture incubator. The resulting formazan blue–colored product was dissolved in 1 ml of acidified isopropanol, and the absorbance was measured at 570 nm by using a SpectraMax Microplate Reader (Molecular Devices Corporation, Sunnyvale, CA).

Determination of DA and its metabolites. Following nanoparticle or metal ion treatment, the cells were homogenized in 0.2 *N* perchloric acid (20% wt/vol) containing an internal standard (3,4-dihydroxybenzylamine; 100 ng/ml). The homogenates were centrifuged at 4°C (13,000 × g; 10 min), and 300 µl of the supernatant was removed and filtered through a 0.45 µm nylon centrifuge tube filter (Costar #8170). Aliquots of 25 µl were injected directly into the HPLC/electrochemical detection system for separation of analytes (Hussain and Ali, 2002). The amount of DA, DOPAC, and HVA were calculated using standard curves that were generated by determining, in triplicate, the ratio between three different known amounts of the amine or its metabolites compared to a constant amount of internal standard.

Dichlorofluorescein assay for ROS. ROS generation was determined using the method described by Wang and Joseph (1999). Viable cells (10^4 per well) were plated into 96-well, collagen-coated plates 1 day before the experiments. On the day of the experiments, after removing the medium, the cells were incubated with 100µM DCFH-DA in the growth medium at 5% CO_2/95% air at 37°C for 30 min. After the DCFH-DA was removed, the cells were washed and exposed to different concentrations of nanoparticles for a period of 24 h. The fluorescence intensity of the cells from each well was measured with a SpectraMax Gemini Plus (Molecular Devices Corporation) microplate reader and recorded with an excitation filter set at 485 nm and an emission filter set at 530 nm. The fluorescence from each well was captured, digitized, and stored on a computer using SOFTmax Pro 3.1.2 (Molecular Devices Corporation). Data were exported to Excel (Microsoft, Seattle, WA) spreadsheet software for further analysis. Data are reported as fold increase in fluorescence intensity relative to the control.

Statistical evaluation. The data were expressed as mean ± SD of three independent experiments. Wherever appropriate, the data were subjected to statistical analysis by one-way ANOVA followed by Dunnett's method for multiple comparisons. A value of $p < 0.05$ was considered significant. SigmaStat for Windows (version 2.03) software was used for the statistical analysis.

RESULTS

Initially, a test was conducted to determine the appropriate solution for the best dispersion of the nanoparticles. From the dispersion tests, the optimal solution for particle dissemination

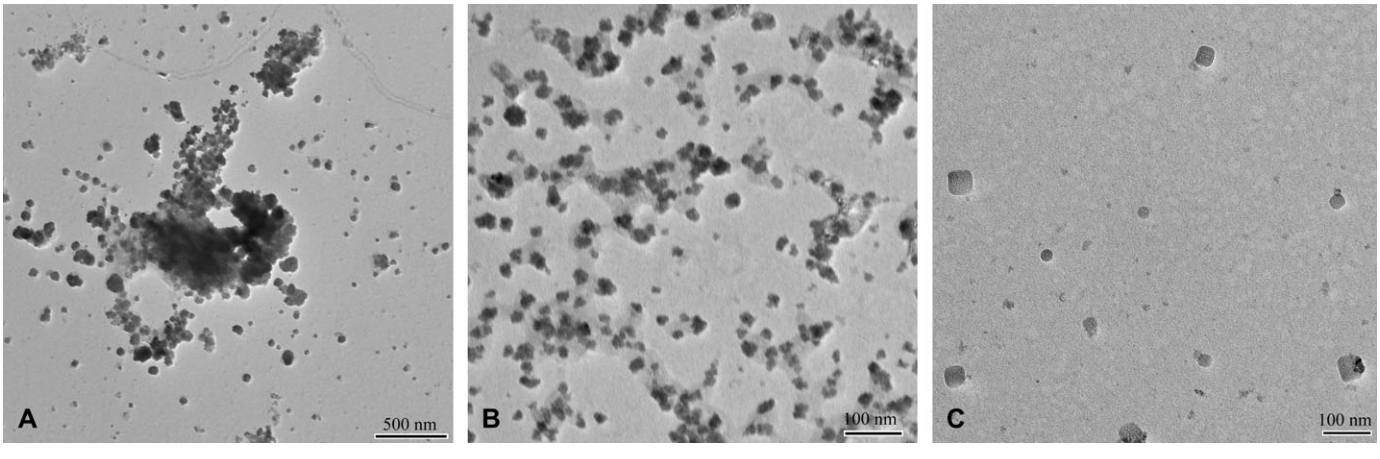

FIG. 2. TEM of Mn-40nm nanoparticles. Mn-40nm nanoparticles were irregularly shaped cubes that tended to agglomerate. (A) Agglomeration of greater than 1 µm in size; (B) relative dispersion of Mn-40nm in some areas on the TEM grid; (C) mean size of 38 nm and an SD of 6 nm calculated from seven individual particles in a random field of view. Scale bars are 500 nm (A), 100 nm (B), and 100 nm (C).

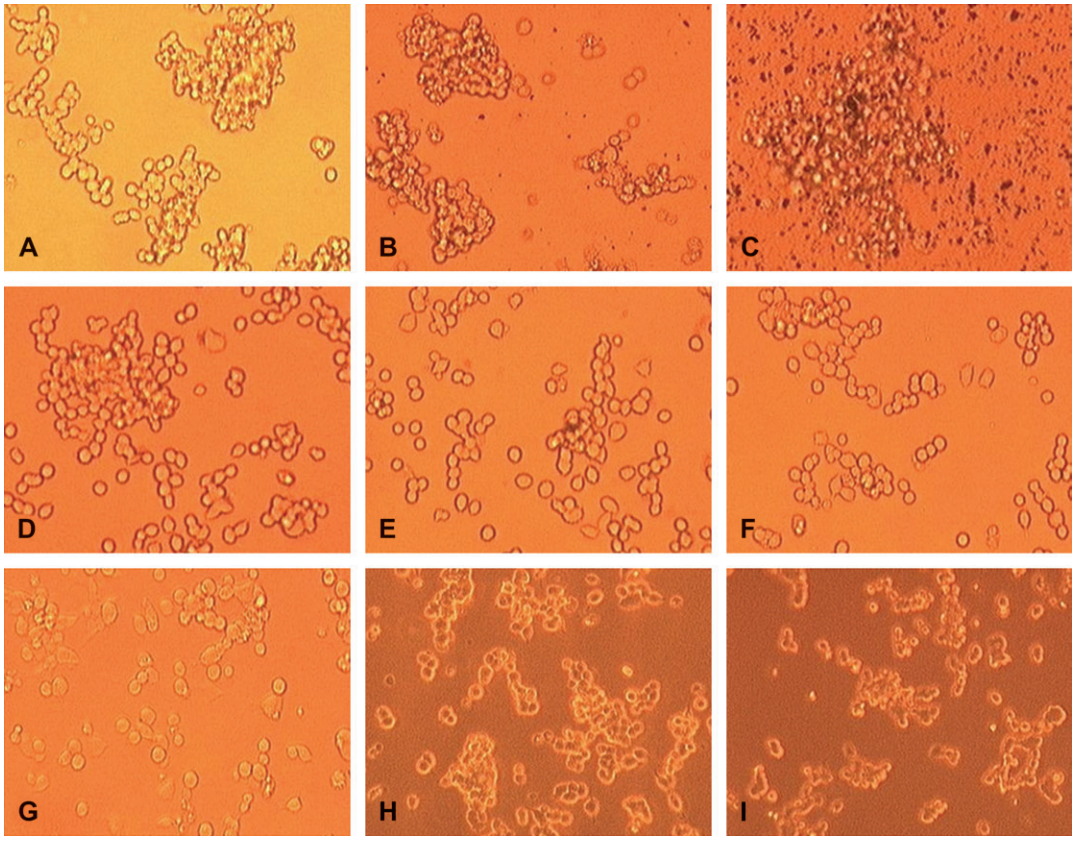

FIG. 3. Cell morphology examined with phase-contrast inverted microscopy. After 24 h of exposure, the morphology of PC-12 cells was observed by phase-contrast microscopy at ×20. (A) Control, (B) Ag-15nm 5 μg/ml, (C) Ag-15nm 50 μg/ml, (D) Mn-40nm 5 μg/ml, (E) Mn-40nm 50 μg/ml, (F) Mn acetate (Mn^{2+}) 5 μg/ml, (G) Mn acetate (Mn^{2+}) 50 μg/ml, (H) $AgNO_3$ 5 μg/ml, and (I) $AgNO_3$ 10 μg/ml. Notice that the cells incubated with Ag-15nm (B, C) or $AgNO_3$ (H, I) appear shrunken with irregular cell borders, whereas control (A), Mn-40nm– (D, E), and Mn^{2+} (F, G)–exposed cells appear relatively similar in size and shape.

was heavily dependent upon the type of particle. Through these tests, we concluded that the optimal medium for Mn-40nm nanoparticles was physiological saline, and deionized water for Ag-15nm nanoparticles. In conducting these tests, we observed the miscibility of nanoparticles in stock solutions, dispersion in culture media both with and without serum, and the pH of the resulting exposure treatment. The pH of both silver and manganese nanoparticles dispersed in exposure media resulted in a consistent pH between 7.0 and 7.4. The solution was turbid with increasing concentrations which is likely to be a result of

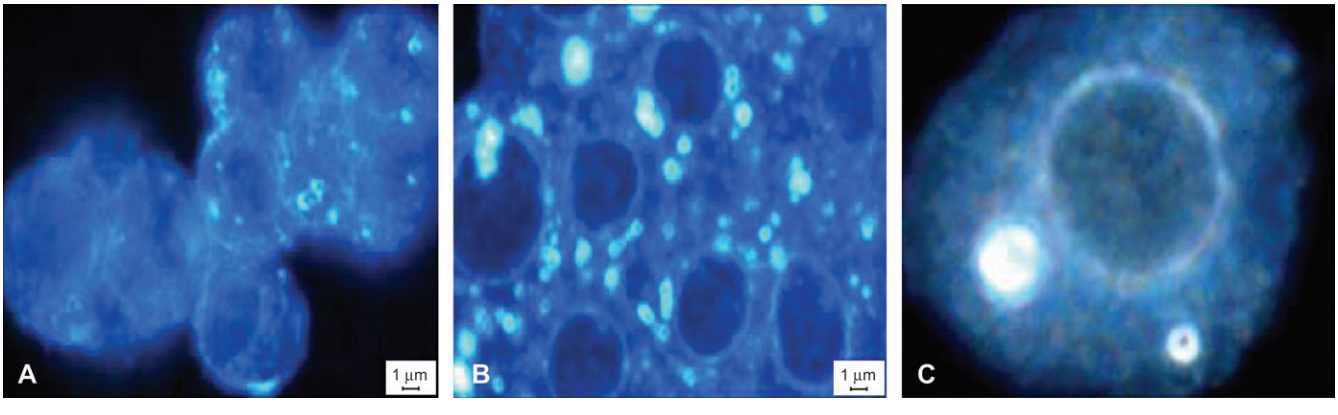

FIG. 4. Uptake and distribution of manganese nanoparticles visualized with high-illuminating inverted microscopy. After 24 h of exposure to a range of Mn-40nm concentrations, cells were washed and examined with the CytoViva150 URI system (×60 magnification). The internalization of Mn nanoparticles was evident in areas of increased brightness within agglomerates of the cells. (A) Control, (B) 50 μg/ml, and (C) 50 μg/ml (single cell enlarged via computer software for clarity).

nanoparticle agglomeration. In order to verify the Mn-40nm nanoparticle size, morphology, dispersion state, and extent of agglomeration, we observed nanoparticle solutions under a microscope equipped with the CytoViva150 URI system for enhanced resolution. Figure 1A shows groups of agglomerated particles in normal physiological solution. However, when 0.1% surfactant (Tween-20) was added, most of the particles appeared to be dispersed (Fig. 1B).

A 1-mg/ml solution of Mn-40nm nanoparticles suspended in water was also examined with bright-field TEM for size, morphology, and dispersion state (agglomeration) as shown in Figures 2A–2C. Some areas of the TEM grid had micrometer-sized Mn agglomerates ranging in size from 1 to over 10 μm. An agglomerate measuring 1.38 μm at ×15,000 is shown in Figure 2A. However, other areas on the TEM grid showed less agglomeration or even individual nanoparticles at magnifications of ×60,000 and ×50,000, respectively (Figs. 2B and 2C). The Mn-40nm nanoparticles were irregular in shape, could readily be measured, and ranged in size from 24.3 to 56.9 nm, with an average size of 38.9 nm and a SD of 11.58 nm taken from 10 individual nanoparticles as shown in Figure 2C. It is possible that the morphologies and agglomeration state of the nanoparticles change with *in vitro* conditions such as incubation in cell culture media and entry into the cells. However, these changes cannot be accurately captured by suspending the materials in water, dispersing them onto a TEM grid, and allowing them to dry before imaging. In this case, the TEM images in Figure 2 only represent the primary particle size of the Mn-40nm as well as nanoparticle aggregation found under these conditions. Therefore, in this respect, the light microscope images provide the strongest evidence for liquid-phase agglomeration that would be most similar to *in vivo* conditions, and the TEM images provide higher magnification data on the primary particle size and shape.

The morphologies of control, Mn-40nm–, Ag-15nm–, and Mn acetate (Mn^{2+})–exposed cells were observed by phase-contrast microscopy (Figs. 3A–3I). Cells treated with Mn-40nm or Mn acetate (Mn^{2+})–exposed cells were not significantly different from control cells. However, cells treated with silver nanoparticles or silver nitrate ($AgNO_3$) appeared to be decreased in size with irregularities in their shape. Therefore, the morphological effect of Mn-based solutions in the same dose (50 μg/ml) as silver-based solutions was less pronounced.

In the present study, the CytoViva150 URI system was also used to follow the uptake, translocation, and distribution of nano-sized Mn particles in PC-12 cells under physiological conditions. Representative images of cells containing Mn-40nm after doses of 50 μg/ml are shown in Figures 4A–4C. These experimental results demonstrate that Mn-40nm nanoparticles and agglomerates are effectively internalized by PC-12 cells. Additionally, bright aggregates were found attached to the outer portions of the cells. As expected, aggregation is an intrinsic property of these particles in solution. Further studies are under investigation to characterize the dynamic properties of these particles/aggregates such as their true size distribution in solution and inside cells.

A significant dose-dependent decrease in mitochondrial function was observed after PC-12 cells were exposed to the nanometals in this study at doses ranging from 10 to 50 μg/ml compared to control, untreated cells (Fig. 5). This result differed from the complete lack of PC-12 mitochondrial function loss after 24 h exposure (data not shown) with 5–100 μg/ml fine carbon black as a positive control particle. However, PC-12 cells displayed a greater mitochondrial toxicity/sensitivity to Mn acetate (Mn^{2+}) compared to Mn-40nm, whereas Ag-15nm was more toxic than both Mn-40nm and Mn^{2+}, confirming the known toxicity of silver. At concentrations of 100 μg/ml, both Mn-40nm and Ag-15nm further reduced the viability of PC-12 cells. When the Mn^{2+} concentration was calculated, it could be considered to approximate the same as the amount administered if Mn nanoparticles were fully solubilized. The Mn^{2+} concentration was approximately 3.2, 8, and 32 μg/ml at doses 5, 10, and 50 μg/ml, respectively. Therefore, based on the MTT assay, Mn-40nm was found to be less toxic than Mn^{2+} or Ag-15nm nanoparticles after incubation with PC-12 cells for 24 h.

The results derived from the DA assay suggest a significant dose-dependent decrease in the levels of DA and its metabolites as a result of exposure to 5- to 50-μg/ml concentrations of Mn nanoparticles or Mn acetate (Mn^{2+}) (Fig. 6) compared to control cells. Mn nanoparticles depleted DA quite similar to Mn^{2+}, whereas Ag-15nm displayed a significant depletion of DA only at a highly toxic dose of 50 μg/ml, which was likely due to loss of cellular function rather than DA pathway disruption (Fig. 6A). DOPAC concentration was significantly depleted in all administered doses (5–50 μg/ml) of Mn-40nm and Mn^{2+} (Fig. 6B). However, with Ag-15nm, there was

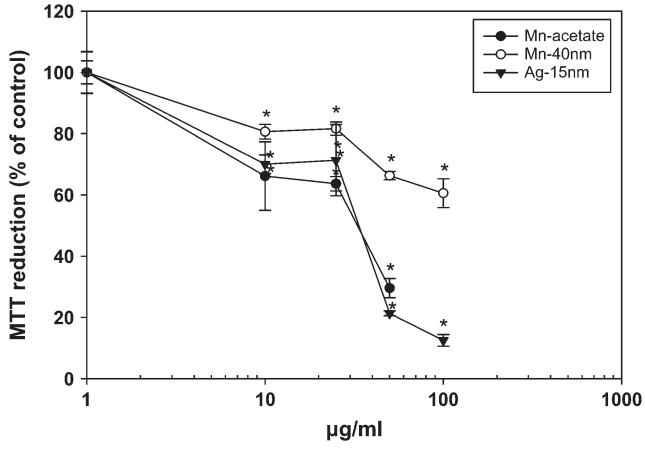

FIG. 5. Effect of nanoparticles on mitochondrial function. After 24 h of exposures, mitochondrial function was determined by the MTT assay as described in the "Materials and Methods" section. Each experimental point is a composite of three independent experiments, with $n \geq 3$ for each point. Statistical significance from control is indicated by asterisk ($p < 0.05$).

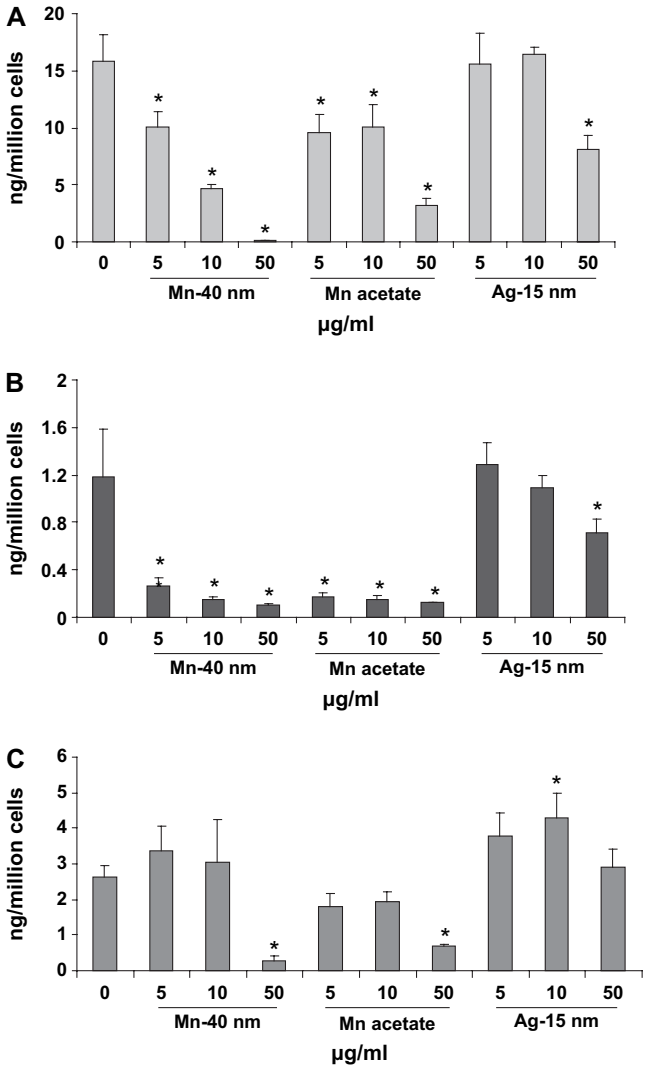

FIG. 6. Effects of nanoparticles on neurotransmitter secretion. After 24 h of exposure, the concentration of neurotransmitters was measured. Each experimental point is a composite of three independent experiments, with $n \geq 3$ for each point. Statistical significance from control is indicated by asterisk ($p < 0.05$). (A) DA; (B) DOPAC; (C) HVA. Both Mn-40nm and Mn acetate (Mn^{2+}) dose dependently decrease DA and its metabolites.

a significant decrease again only at the 50 µg/ml dose (Fig. 6B). There were no significant changes in HVA levels after the cells were incubated with concentrations ranging from 5 to 10 µg/ml of Mn-40nm or Mn^{2+}, while there were significant depletions of HVA at doses of 50 µg/ml for both Mn-based solutions.

The ROS levels were measured to examine the involvement of oxidative stress in Mn-40nm toxicity (Figs. 7A–7C). It appears that Mn-40nm induces a 10-fold or greater increase in ROS levels, whereas Mn acetate (Mn^{2+}) and Ag-15nm only induce a threefold or greater increase in ROS levels relative to the basal control levels. Therefore, the production of ROS in PC-12 cells incubated with Mn-40nm is much higher than both Mn^{2+}- and Ag-15nm–exposed cells.

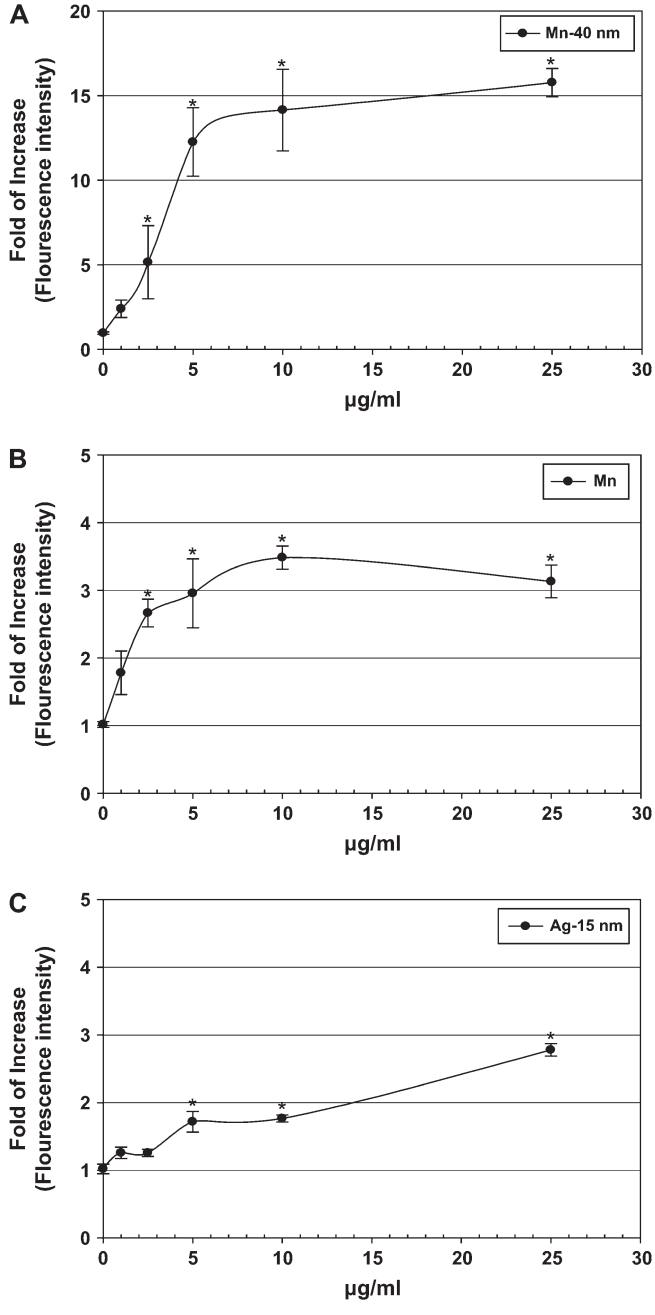

FIG. 7. Effect of nanoparticles on ROS generation in PC-12 cells. After incubation with DCFH-DA for 30 min, washing, and exposure with nanoparticles for 24 h, fluorescence was measured with a microplate reader as described in the "Materials and Methods" section. The intensity of fluorescence is expressed as the fold increase in treated cells with respect to control. The data are expressed as means ± SDs of three experiments. Asterisk indicates a statistically significant difference compared to controls ($p < 0.05$). (A) Mn-40nm, (B) Mn acetate (Mn^{2+}), and (C) Ag-15nm. There was a 10-fold or greater increase in ROS after incubation with Mn-40nm compared to an approximately threefold or greater increase for Mn acetate (Mn^{2+}) or Ag-15nm.

DISCUSSION

Despite the many applications of nanomaterials, some studies indicate that certain nanoparticles may adversely affect human health due to their small size, reactive properties, and high surface area to material amount/weight. Indeed, their small size and large surface area may allow them to readily gain entry into cells and tissues. Some nanoparticles may enter through inhalation, into the nose or lungs, or through ingestion, entering the digestive system. Once in the body, due to their minute size, nanoparticles may translocate to sites distant from their portal of entry (Oberdorster *et al.*, 2005). Such translocation is facilitated by the propensity of nanoparticles to enter cells, cross cell membranes, and move within or along the axons and dendrites that connect neurons. Nanoparticles have been shown to enter the brain via the *nervus olfactorius* after deposition on the olfactory mucosa of the nose following instillation or inhalation (Oberdorster *et al.*, 1995). This preferential toxicodynamic distribution of nanoparticles in the nasal passage increases the CNS entry potential and the potential for metal particulate toxicity to sensitive neurons within the CNS.

This study was designed to evaluate whether nanoscale particles (< 100 nm), such as Mn-40nm and Ag-15nm, induced toxicity in a neuroendocrine cell line (PC-12) when compared to the known neurotoxin manganese ion (Mn^{2+}). For toxicity evaluations, cellular morphology, mitochondrial function (MTT assay), and DA/its metabolites were assessed at 24 h after exposure to doses of nanoparticles or metal ions and compared to unexposed cells. PC-12 cells have been used as an *in vitro* model system to demonstrate that submicromolar concentrations of Mn^{2+} induce extracellular DA depletion (Alinovi *et al.*, 1996). Manganese (Mn) is an essential element in brain development (Hurley, 1981), but it can be toxic and lead to neurological symptoms mimicking parkinsonism. Manganese induces neurotoxicity by interacting with basal ganglia, selectively depleting striatal DA (Archibald and Tyree, 1987), and generating oxidative stress (Hussain *et al.*, 1997; Simonian and Coyle, 1996), which may play an important role in Mn-induced neuronal degeneration. However, it is not yet known whether Mn nanoparticles produced effects similar to their soluble counterpart manganese ion (Mn^{2+}) *in vivo*.

The most important characteristics of nanoparticles are their size, surface area, and reactivity. One property of nanoparticles not well considered in toxicity, but well considered for therapeutic use, is the dissolution of materials after delivery into the cells. Therefore, in addition to the ease of entry and immense surface areas delivered in a dose, soluble metal ionic species could be released over time from intracellular or tissue accumulations acting as toxic reservoirs. This would make the nanoparticles exhibit other dramatically different biological characteristics compared to their soluble metal counterparts. If this is the case, then these nanoparticles may elude mechanisms that would otherwise protect cells such as membrane pumps that would not allow high concentrations of metal ions to exist in the cells. If the protective cellular mechanisms are left unchecked because of the gradual metal ion release, the resulting accumulation of toxic metal ions may cause progressive cytotoxicity and tissue pathophysiology. In these studies, large amounts of agglomerated Mn-40nm particles were found both inside and outside of the cells, suggesting that much of the material remained in the agglomerated form. These agglomerates could contribute to such a scheme, but this has yet to be explored.

The results from the current study demonstrated that Mn ions are significantly toxic at the 10-μg/ml dose, whereas Mn-40nm nanoparticles are only moderately toxic at the same dose. Additionally, both Mn-40nm and Mn acetate (Mn^{2+}) deplete the levels of DA and its metabolites in a dose-dependent manner. Therefore, it can be concluded that both forms of Mn act in very much the same manner with regards to PC-12 toxicity and neurotransmitter function. However, it is unclear whether longer exposure times with Mn-40nm nanoparticles may further increase their toxicity or deplete DA/its metabolites compared to Mn^{2+}.

The DA depletion induced by Mn-40nm and Mn^{2+} was also compared with another nanoparticle, Ag-15nm, known to exhibit toxicity in other cell lines (Braydich-Stolle *et al.*, 2005; Hussain *et al.*, 2005). Our previous results indicated that Ag-15nm can induce toxicity, in part, through oxidative stress in liver cells (Hussain *et al.*, 2005). In this study, our results show that Ag-15nm did not deplete DA except at a high and cytotoxic dose (50 μg/ml). It is clear that both Mn-40nm and Mn^{2+} induced DA depletion and caused a reduction in its metabolites in a dose-dependent manner (Fig. 6). Our results also clearly demonstrated that Mn-40nm induced ROS at significantly greater amounts compared to Ag-15nm or Mn^{2+}. It is possible that the increased production of ROS could be due to the generation or direct interaction of oxidized DA metabolites with DCFH-DA. Other studies have shown that manganese ions can directly oxidize monoamines such as serotonin and DA (Lloyd, 1995; Segura-Aguilar and Lind, 1989) or that the products of monoamine oxidation may covalently link to serotonin-binding protein (Velez-Pardo *et al.*, 1997, 1998). It is currently unknown whether Mn-40nm selectively interferes with DA metabolism through ROS production, depletion of DA by interfering with metabolic pathways/select enzymes (tyrosine hydroxylase) involved in DA synthesis, or through the direct oxidation of DA metabolites. There may be both enzymatic (e.g., tyrosine hydroxylase inhibition) and nonenzymatic (direct oxidation) mechanisms that may underlie these reductions in cellular DA and DA metabolite levels (Almas *et al.*, 1992). However, this significant increase in ROS is noteworthy and is under further investigation.

Manganese is a well-recognized neurotoxin that produces symptoms such as diminished motor skills and psychological disturbances, which parallel those of Parkinson's disease. Due to large volume of industrial applications for Mn metal, it is

anticipated that newly developed Mn nanoparticles will be utilized in many similar applications, possibly even replacing bulk Mn metal in the near future. However, it is still not clear whether nano-sized Mn materials can produce symptoms similar to soluble Mn or from Mn macroparticles *in vivo*. However, our preliminary data show quite remarkably that DA and its metabolites are substantially depleted, which is a major target for Mn toxicity. These results are not specific to the nano-size of the particles because the positive control, Ag-15nm, although toxic, did not reduce DA and its metabolites in the same manner or produce the same level of ROS production as Mn-40nm nanoparticles or Mn acetate (Mn^{2+}) solutions. Collectively, these data suggest that DA depletion is a specific effect of Mn nanomaterial, although there were variations in the degree of toxicity, neurotransmitter depletion, and ROS production, with Mn-40nm nanoparticles appearing less toxic and producing much larger quantities of ROS compared to Mn^{2+}. Nonetheless, the extent to which the dramatic effect of manganese on DA neurotransmitters, observed here, extrapolates to animals or humans remains to be shown. Presently we are evaluating the depletion of DA by Mn-40nm in an animal model to assess if these nanoparticles can cross the blood-brain barrier or gain entry into the brain through the olfactory bulb neuroprocesses.

ACKNOWLEDGMENTS

The authors would like to thank Col James R. Riddle for his strong support and encouragement for this research, Dr Gunter Oberdörster for supplying the Mn nanomaterial and for his helpful comments during the setup of this work, and Dr William Slikker for his help in establishing work between laboratory teams. A.M.S. was funded under an award from the Dayton Area Graduate Studies Institute fellowship grant. A.J. was funded by the Biosciences and Protection Division, Air Force Research Laboratory under Oak Ridge Institute for Science and Education, Oak Ridge, TN.

REFERENCES

Alinovi, R., Vettori, M. V., Mutti, A., Cavazzini, S., Bacchini, A., and Bergamaschi, E. (1996). Dopamine (DA) metabolism in PC12 cells exposed to manganese (Mn) at different oxidation states. *Neurotoxicology* **17,** 743–750.

Almas, B., Le Bourdelles, B., Flatmark, T., Mallet, J., and Haavik, J. (1992). Regulation of recombinant human tyrosine hydroxylase isozymes by catecholamine binding and phosphorylation. Structure/activity studies and mechanistic implications. *Eur. J. Biochem.* **209,** 249–255.

Aschner, M., Erikson, K. M., and Dorman, D. C. (2005). Manganese dosimetry: Species differences and implications for neurotoxicity. *Crit. Rev. Toxicol.* **35,** 1–32.

Archibald, F. S., and Tyree, C. (1987). Manganese poisoning and the attack of trivalent manganese upon catecholamines. *Arch. Biochem. Biophys.* **256,** 638–650.

Braydich-Stolle, L., Hussain, S., Schlager, J., and Hofmann, M. C. (2005). In vitro cytotoxicity of nanoparticles in mammalian germ-line stem cells. *Toxicol. Sci.* **88,** 412–419.

Carmichael, J., Degraff, W. G., Gazdar, A. F., Minna, J. D., and Mitchell, J. B. (1987). Evaluation of a tetrazolium-based semi-automated colorimetric assay: Assessment of chemo sensitivity testing. *Cancer Res.* **47,** 936–942.

Cui, D., and Gao, H. (2003). Advance and prospect of bionanomaterials. *Biotechnol. Prog.* **19,** 683–692.

Furno, F., Morley, K. S., Wong, B., Sharp, B. L., Arnold, P. L., Howdle, S. M., Bayston, R., Brown, P. D., Winship, P. D., and Reid, H. J. (2004). Silver nanoparticles and polymeric medical devices: A new approach to prevention of infection? *J. Antimicrob. Chemother.* **54,** 1019–1024.

Han, M. J., Ozaki, T., and Yu, J. (2005). Electronic structure and magnetic properties of small manganese oxide clusters. *J. Chem. Phys.* **123,** 34306.

Hurley, L. S. (1981). The roles of trace elements in foetal and neonatal development. *Philos. Trans. R. Soc. Lond. B. Biol. Sci.* **294**(1071), 145–152.

Hussain, S., and Ali, S. F. (2002). Zinc potentiates 1-methyl-4-phenyl-1,2,3,6-tetrahydropyridine induced dopamine depletion in caudate nucleus of mice brain. *Neurosci. Lett.* **335,** 25–28.

Hussain, S., Slikker, W., Jr, and Ali, S. F. (1997). The effects of chronic exposure of manganese on antioxidant enzymes in different regions of rat brain. *Neurosci. Res. Commun.* **21,** 135–144.

Hussain, S. M., Hess, K. L., Gearhart, J. M., Geiss, K. T., and Schlager, J. J. (2005). In vitro toxicity of nanoparticles in BRL 3A rat liver cells. *Toxicol. In Vitro* **19,** 975–983.

Jayakumar, A. R., Rama Rao, K. V., Kalaiselvi, P., and Norenberg, M. D. (2004). Combined effects of ammonia and manganese on astrocytes in culture. *Neurochem. Res.* **11,** 2051–2056.

Lam, C. W., James, J. T., McCluskey, R., and Hunter, R. L. (2004). Pulmonary toxicity of single-wall carbon nanotubes in mice 7 and 90 days after intratracheal instillation. *Toxicol. Sci.* **77,** 126–134.

Lloyd, R. V. (1995). Mechanism of the manganese-catalyzed autoxidation of dopamine. *Chem. Res. Toxicol.* **8,** 111–116.

Monteiro-Riviere, N. A., Nemanich, R. J., Inman, A. O., Wang, Y. Y., and Riviere, J. E. (2005). Multi-walled carbon nanotube interactions with human epidermal keratinocytes. *Toxicol. Lett.* **155,** 377–384.

Oberdörster, E. (2004). Manufactured nanomaterials (fullerenes, C60) induce oxidative stress in the brain of juvenile largemouth bass. *Environ. Health Perspect.* **112,** 1058–1062.

Oberdorster, G., Gelein, R. M., Ferin, J., and Weiss, B. (1995). Association of particulate air pollution and acute mortality: Involvement of ultrafine particles? *Inhal. Toxicol.* **7,** 111–124.

Oberdorster, G., Oberdorster, E., and Oberdorster, J. (2005). Nanotoxicology: An emerging discipline evolving from studies of ultrafine particles. *Environ. Health Perspect.* **113,** 823–839.

Olanow, C. W. (2004). Manganese-induced parkinsonism and Parkinson's disease. *Ann. N. Y. Acad. Sci.* **1012,** 209–223.

Segura-Aguilar, J., and Lind, C. (1989). On the mechanism of the $Mn^3(+)$-induced neurotoxicity of dopamine: Prevention of quinone-derived oxygen toxicity by DT diaphorase and superoxide dismutase. *Chem. Biol. Interact.* **72,** 309–324.

Simonian, N. A., and Coyle, J. T. (1996). Oxidative stress in neurodegenerative diseases. *Annu. Rev. Pharmacol. Toxicol.* **36,** 83–106.

Velez-Pardo, C., Jimenez Del Rio, M., Verschueren, H., Ebinger, G., and Vauquelin, G. (1997). Dopamine and iron induce apoptosis in PC12 cells. *Pharmacol. Toxicol.* **80,** 76–84.

Velez-Pardo, C., Del Rio, M. J., Ebinger, G., and Vauquelin, G. (1998). Monoamine and iron-related toxicity: From "serotonin-binding proteins" to lipid peroxidation and apoptosis in PC12 cells. *Gen. Pharmacol.* **31,** 19–24.

Wang, H., and Joseph, J. A. (1999). Quantitating cellular oxidative stress by dicholorofluorescein assay using microplate reader. *Free Radic. Biol. Med.* **27,** 612–616.

Wu, X., and Bruchez, M. P. (2004). Labeling cellular targets with semiconductor quantum dot conjugates. *Methods Cell Biol.* **75,** 171–183.